Journal of
Renewable Energy Research and Applications (RERA)

Vol 2. No 1, 2021, 9-23 *DOI: 10.22044/RERA.2020.9998.1038*

Energy, Exergy, and Economic Analyses and Optimization of Solar Organic Rankine Cycle with Multi-objective Particle Swarm Algorithm

A.Beiranvand[1], M. A. Ehyaei[1*], A. Ahmadi[2] , José Luz Silveira[3]

1. Department of Mechanical Engineering, Pardis Branch, Islamic Azad University, Pardis New City, Iran.
2. School of New Technologies, Iran University of Science & Technology, Islamic Republic of Iran.
3. Sao Paulo State University, UNESP, FEG, Energy Department, Brazil

Receive Date 07 June 2019; Revised Data 25 June 2019; Accepted Date 27 June 2019
* *Corresponding author: aliehyaei@yahoo.com (M. A.Ehyaei)*

Abstract
The high potential of solar energy in Iran as well as the problem of air pollution makes it increasingly inevitable that solar energy is used. In this work, the solar-powered organic Rankine cycle (ORC) is investigated. A solar-type collector is a flat plate collector. The energy, exergy, and economic analyses of the hybrid system with the MOPSO algorithm are carried out for Tehran, the capital of Iran. The working fluid of the solar collector is assumed to be water, and the working fluid of ORC is R123. The MATLAB software is used for the simulation, and to compute the R123 fluid properties, the Refprop software is used. The exergy investigation shows that the most exergy destruction is related to the evaporator. Two objective functions consisting of the exergy efficiency and the price of electricity are considered. The decision variables for this optimization are considered as the number of solar collector panels and the pumps, the turbine isentropic efficiency, and the pressures of the condenser and the evaporator. The Pareto diagram shows that the exergy efficiency of the system can vary in the range of 7.5-10.5 %, and the price of the produced electricity can vary in the range of 0.2-0.26 $/kWh.

Keywords: *Exergy, Organic Rankine cycle, Flat collector, Energy, Economic, Solar.*

1. Introduction
The lack of fossil fuel and the gradual rise in its price as well as the environmental pollution and the increase in the global warming have caused the progress and usage of renewable energy as a major priority [1-3]. Among the solutions and technologies available in the renewable energy resources, the application of Organic Rankine Cycle (ORC) plays a significant role. The following benefits can be summarized for ORC [4-6]:

- The ORC technology is available to convert the low-temperature renewable energy resources such as geothermal, solar, and biomass into the electrical energy.
- Owing to the heat recovery of the waste heat generated in the industries, the need for energy can decrease affectedly.
- By applying ORC to the combined heating and power generation systems, a share of energy request for the buildings can be provided by these technologies.
- Application of solar ORC with absorption chiller (the hybrid system in this work) can supply all the electrical, heating, and cooling loads of a system by a minimum environmental impact and clean energy.

The shortage of fossil fuels, increasing the cost, and raising concerns about global warming are the major problems for fossil fuels. The solutions such as using the ORC technology powered by renewable energies are the key factors. The application of ORC to convert waste heat to useful power has been examined in different research works [7-9]. The usage and application of ORC systems have been conducted in some other studies [10, 11]. Numerous research works have been reported regarding the selection of the best working fluid in ORC [9,12].
Roy et al. [13] have examined the application of ORC with regenerator at the constant pressure and superheat condition for the two working fluids of R123 and R134. In this study, the efficiency, net output work of the turbine, overall irreversibility,

and second law efficiency of the cycle were obtained based on the constant and variable temperatures of the reservoir. As a result, the working fluid R123 was introduced as the best working fluid for this ORC.

Wang et al. [14] have optimized 13 different types of working fluids in ORC by the simulated annealing algorithm. In this study, the optimal parameters of ORC and the effects of the reservoir temperature, pinch temperature variations, and economic parameters on the ORC performance were also calculated. The results obtained revealed that the choice of working fluid had the highest effect on the performance of the cycle. Other similar research works have also been performed by the other researchers [15-17].

Moreover, the usage of different working fluids in ORC has been studied in other research works [18,19].

Also the application of the multi-component fluid for ORC has been examined [20-22]. Also the optimization of the multi-component working fluid has been performed [23,24].

Karellas et al. [25] have investigated the heat transfer performance of the supercritical fluid in the flat plate heat exchanger. They concluded that by increasing the efficiency of ORC, the cost of ORC was increased too.

Chen et al. [26] have compared R32 and CO2 as the working fluids of ORC at the supercritical condition to convert low-temperature waste heat into useful power. The results obtained showed that although CO2 was plentiful, inflammable, non-toxic, and cheap, the thermodynamic performance and operational pressure of this gas was poor in comparison with R32.

In another study, Chen et al. [27] have compared ORC with a Zeotropic mixture of 0.3 R32 and 0.7 R134a in the supercritical condition and pure R134 in the same conditions as the working fluid at the same temperature. The results obtained revealed that the efficiency of the zeotropic mixture as the working fluid varied from 10.8% to 13.3%.

Wang et al. [28] have examined the combined ORC and cooling systems, whereas R245fa as the working fluid of ORC and R134a was as the working fluid of the cooling system. In this combined system, these two systems were coupled by a shaft using a high efficiency microchannel and scroll expander heat exchanger. This configuration was designed with low weight and capacity to cool down an engine of the automobile.

Wang et al. [29] have analyzed the thermodynamic and optimal conditions of ORC powered by the solar energy. The results of this study showed that this cycle by R245fa and R123 as the working fluid had a better efficiency.

Baccioli et al. [30] have investigated the solar parabolic collector and ORC in a dynamic model. The assessment performance of ORC over a year showed that this system had a good performance without a reservoir.

Bello and Tzivanidis [31] have examined ORC with the solar energy. The results obtained showed that based on 150-300 oC as the temperature of the resource and toluene as the working fluid, the amount of 400-880 kWh of electricity could be produced.

The cogeneration system with the application of ORC has been testified in several studies. Saadatfar et al. [32] have presented a system of combined power, heating, and cooling generation with solar energy using a nano-fluid as a working fluid. The results obtained showed that adding the nanoparticles of pentane silver to the working fluid was a suitable alternative as a working fluid.

Mokhtari et al. [33] have investigated the hybrid systems of water treatment systems using reverse osmosis, parabolic trough solar collector, and ORC. This system was applied for the city of Mar Kola in the north of Iran. The fresh water produced by this system was about 4000 m3/day.

Zhang et al. [34] have investigated a combination of the solar cycle and ORC to produce power, heating, and cooling of a residential place. The energy analysis of this combination was succeeded. The results obtained revealed that this combination fulfilled the needs of the case study during a year. Similar research works have been carried out by Patel et al. [35] and Mohammadi et al. [36]. Several types of research works exist in the literature about the cogeneration system with residential applications [37-41].

Based on the mentioned literature, it is clear that the feasibility study and optimization of solar ORC are a relatively novel idea.

In this research work, a combination of ORC and a flat plate solar collector was applied to generate electricity, heating, and cooling. In this study, the energy, exergy, and economic analyses of ORC with flat plate collectors were carried out. This study was done based on the weather and solar conditions in Tehran. By considering the decision variables, the optimization of two functions consisting of electricity cost and exergy efficiency was carried out based on the MOPSO algorithm.

The innovations of this article are as follow:

- Feasibility study of the application of solar ORC for Tehran (Iran) based on the energy, exergy, and economic analyses;

- Two-objective (exergy and electricity cost) optimization of ORC performed by the MOPSO algorithm;
- Sensitivity analysis of the ORC system based on different decision variables.

2. Mathematical modeling

A schematic representation of the system is shown in figure 1.

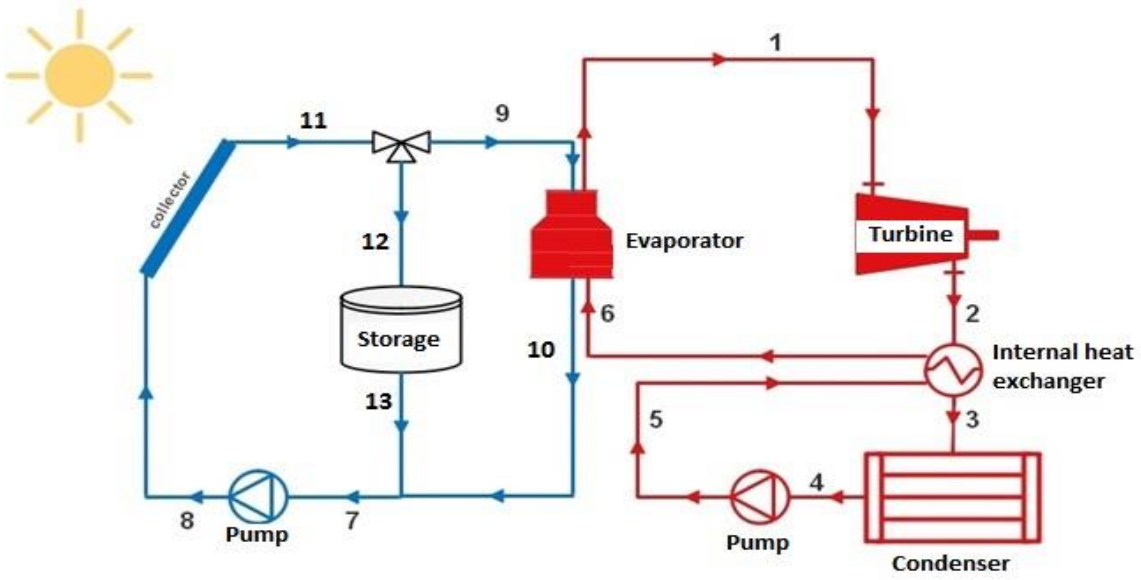

Figure 1. A schematic diagram of the case study.

As shown in this figure, the absorbed energy by the sun enters an intermediate fluid (water), and then this energy is transferred to the operational fluid at the evaporator of ORC. In ORC, the working fluid of ORC in a superheat condition enters the turbine or expander (point 1). Thus the energy is transferred to the shaft, and a power is produced. Then the working fluid can come out of the turbine in a superheat state (point 2). This working fluid passes through a heat exchanger as a regenerator, and the heat is taken from this part and transferred to the operational fluid, entering the evaporator. Thus the working fluid leaves the regenerator in a saturated vapor (point 3). Then this fluid passes through the condenser, losses the heat, and leaves the condenser as a saturated liquid. Thus by passing through the pump, the pressure of the working fluid rises. Then it enters the internal heat exchanger (regenerator), and the working fluid heats up by taking heat from the extracted fluid of the turbine. As a result, its temperature is increased, and hence, the efficiency of the system is increased too. Finally, this ORC working fluid enters the evaporator to gain heat from the intermediate fluid flow of the solar collector. Therefore, this cycle is repeated over time.

The case study of this research work was Tehran. The city is extended in the longitudinal ranges of 51 degrees and 2 minutes, eastern to 51 degrees and 36 minutes, and eastern over 50 km. Its latitude ranges from 35 degrees and 35 minutes of the north to 35 degrees and 50 minutes over 30 km. The temperature of the environment was determined as one of the decision variable parameters during the day and in the different months according to the reference. The average monthly ambient temperature and wind speed of Tehran are given in table 1 for different months [42].

An important parameter in a solar energy system is the solar radiation (Figure 2). Based on the

Table 1. Daily average temperature of Tehran from 1951 to 2010 for different months.

Months	Jan	Feb	Mar	Apr	May	June	Jul	Aug	Sep	Oct	Nov	Dec
Temp (°C)	8.3	6.0	10.7	16.8	22.1	27.5	30.3	29.5	25.5	19.0	11.6	5.9
Wind speed (m/s)	4.5	5.2	5	5.6	5.9	5.4	4.5	4	3.8	4.2	4.8	3.6

reference [24], the amount of the radiation intensity in Tehran can be observed over a year.

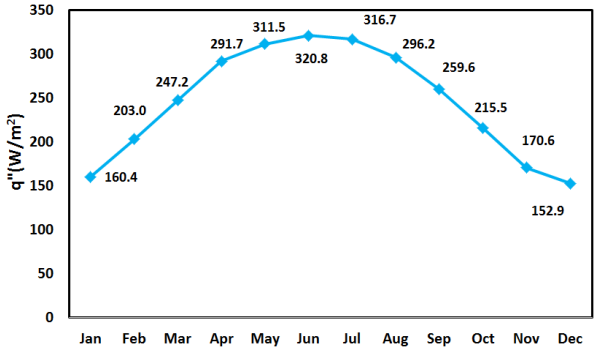

Figure 2. Average solar radiation in Tehran over a year [24].

The specifications of a solar flat collector and storage tank are shown in table 2.

Table 2. Specifications of a solar flat collector.

No.	Specification	Uint	Value
1	Length of flat plate solar collector	m	1.57
2	Width of flat plate solar collector	m	0.8
3	Number of pipes	-	80
4	Diameter of pipes	m	0.127
5	Storage tank volume	m^3	1
6	ε_p	-	0.96
7	ε_a	-	0.96

The rate of the absorbed energy by the solar flat plate collector is obtained by the following equations [43]:

$$S = I_b R_b (\tau\alpha)_b + I_d (\tau\alpha)_d \frac{(1+\cos\beta)}{2} + (I_b + I_d)(\tau\alpha)_g \rho_g \frac{(1+\cos\beta)}{2} \quad (1)$$

In equation (1), the indices b, d, and g are due to the direct radiation, scattered radiation from the sky, and scattered radiation due to the reflection of the ground surface. I is the intensity of radiation on the horizontal surface by considering the effect of the environment dust, which is calculated based on the Reference [44].

The constant values that are determined by the experimental results are multiplied by the amount of radiation intensity, and ultimately, the amount of these quantities is determined. Moreover, τα is the transmission absorption coefficient, β is the solar collector slope, and ρ_g is the reflection coefficient of the Earth's surface that it is equal to 0.93. R_b is a dimensionless parameter, and represents the scattered radiation of the sky, and is expressed as follows [43,44]:

$$R_b = \frac{\cos\theta}{\cos\beta} \quad (2)$$

In this case, ɵ is the angle of the sunlight with the collector surface. The scattered radiation is calculated as follows [43]:

$$\frac{I_d}{I_t} = \begin{cases} 1 - 0.09k_T & k_T < 0.22 \\ 0.9511 - 0.1604k_T + 4.388k_T^2 & 0.22 < k_T < 0.8 \\ -16.638k_T^2 + 12.336k_T^4 & 0.165k_T > 0.8 \end{cases} \quad (3)$$

In this case, k_T is dimensionless, and is the average monthly clearance coefficient.

The general heat loss of the collector is obtained by the following equation [43]:

$$\dot{Q}_{Loss} = U_L A(T_p - T_a) \quad (4)$$

In the above equation, U_L is the total heat transfer coefficient, A is the collector area, and Ta is the ambient temperature. In order to obtain the total heat transfer coefficient, the following relationship exists [43]:

$$U_L = U_t + U_b + U_e \quad (5)$$

U_e and U_b are the total heat transfer from the sides and the bottom, respectively, and U_t is the overall heat transfer coefficient from above the collector, which is calculated by the following equation [43].

$$U_t = \frac{C}{T_p}\left(\frac{T_p - T_a}{1+f}\right)^{0.33} + \frac{1}{h_w} + \frac{\sigma(T_p^2 + T_a^2)(T_p + T_a)}{\frac{1}{\varepsilon_p} + 0.05(1+\varepsilon_p) + \frac{1+f}{\varepsilon_c} - 1} \quad (6)$$

In the above equation, h_w=2.6 + $3V_{wind}$ is the forced heat transfer coefficient between the glass cover exposed to ambient air, which is determined in terms of wind speed (V_{wind}). Also ε_p and ε_C are the diffusion coefficients for the absorption plate and the glass cover for infrared radiation, respectively. Also σ is the Stephen Boltzmann's constant. The parameters C and f are calculated by the following equations [43]:

$$C = 365.9(1 - 0.00883\beta + 0.0001298\beta) \quad (7)$$

$$f = 1.091(1 - 0.04h_w + 0.0005h_w) \quad (8)$$

β is the solar collector slope. The amounts of U_e and U_b are calculated as follow [43]:

$$U_b = \frac{k_b}{L_b} \quad (9)$$

$$U_e = \frac{k_e}{L_e} \quad (10)$$

In the above equations, L_b and k_b are the width

and thermal conductivity coefficients of the insulation plate located below the absorbent plate, respectively. Also Le and k_e are the thickness and thermal conductivity coefficient insulation plate that is located on the sides of the absorbent plate. The useful heat gain rate and plate temperature are calculated by the following equations [43]:

$$\dot{Q}_{SC} = AF_R\big(I_t(\tau\alpha) - U_L(T_i - T_a)\big) \quad (11)$$

$$T_p = T_i + \frac{\dot{Q}_{SC}}{AF_R U_L}(1 - F_R) \quad (12)$$

It, τα, T_i, and A are the direct radiation flux on the slope plate, transmission absorption coefficient, temperature of the fluid to the collector, and collector area, respectively. Also, F_R is the harvesting factor of the collector, and it is calculated by the following equation [43]:

$$F_R = \frac{\dot{m}Cp}{AU_L}\left[1 - e^{-\left(\frac{U_L F' A}{\dot{m}Cp}\right)}\right] \quad (13)$$

In this equation, $\dot{m}$ and Cp are the mass flow rates of water entering the collector and specific heat at a constant pressure of water, respectively. Also F' is an efficiency coefficient of the collector, which is calculated by the following equation [43]:

$$F' = \frac{\frac{1}{U_L}}{W\left[\frac{1}{U_L(D_o + W - D_o)F} + \frac{1}{C_b} + \frac{1}{\pi D_i h_{fi}}\right]} \quad (14)$$

In the above relation, W, D_i, and D_o are the distance between the pipes in the collector, inner diameter, and outer diameter of the fluid tube. Also C_b = 0.027 and h_{fi} are the conduction coefficients of the substances that connect the tube to the absorber plate and the heat transfer coefficient of fluid, respectively. The last parameter is calculated according to the Chininskian relation[45]. The energy conservation equations for ORC are in table 3[45].

Table 3. Conservation of energy equation energy and exergy for ORC.

No.	Equipment	Energy Equation
1	Pump	$\dot{W}_p = \dot{m}_1(h_5 - h_4)$
2	Evaporator	$\dot{Q}_E = \dot{m}_5(h_1 - h_6)$
3	Condenser	$\dot{Q}_C = \dot{m}_1(h_3 - h_4)$
4	Internal heat exchanger	$\dot{Q}_{IHE} = \dot{m}_2(h_3 - h_2) = \dot{m}_5(h_6 - h_5)$
5	Turbine	$\dot{w}_T = \dot{m}_1(h_1 - h_2)$

In the table above, $\dot{m}$ is the fluid mass flow rate, $\dot{W}$ and $\dot{Q}$ are the rates of output work and heat transfer, respectively, and h (J⁄kg) is the enthalpy. Also the sub-titles P, T, C, E, and IHE represent the pump, turbine, condenser, evaporator, and internal heat exchanger, respectively. The points are also shown in figure 1.

Also the heat transfer rate of the solar collector can be obtained by the following equation [45]:

$$\dot{Q} = U \cdot A \cdot LMTD \quad (15)$$

where U, A, and LMTD are the heat transfer coefficient, area of the heat exchanger, and logarithmic mean temperature difference, respectively [45].

The logarithmic mean temperature difference is defined as:

$$LMTD = \frac{\Delta T_A - \Delta T_B}{\ln(\frac{\Delta T_A}{\Delta T_B})} \quad (16)$$

In this model, the reservoir tank is a storage tank with water fluid. The returned fluid from the collector and the fluid entering from the hot water are completely mixed. The heat loss of the storage tank is calculated based on the defined efficiency (η_{TST}) by the Reference [46].

Therefore, by uniformly assuming the fluid temperature in the tank and neglecting the potential and kinetic energy, the energy conservation to the storage tank is calculated as follows [46]:

$$mC_p\frac{dT}{dt} = \eta_{TST}(\dot{Q}_{net}) \quad (17)$$

where T is the mean temperature of the storage tank, m is the stored mass inside the tank, t represents the time, and $\dot{Q}_{net}$ is the net heat transfer of the tank.

Exergy can be separated into four parts. The physical exergy and chemical exergy are two important types of exergy. In this work, the two components of kinetic exergy and potential exergy are neglected. By application of the first and second laws of thermodynamics, the following exergy equilibrium is found [47-50]:

$$\dot{E}x_Q + \sum_i \dot{m}_i ex_i = \sum_e \dot{m}_e ex_e + \dot{E}x_W + \dot{E}x_D \quad (18)$$

where $\dot{E}x_Q$, $\dot{m}_i$, and ex_i are the heat transfer exergy flow, inlet mass flow rate, and specific exergy for i stream. Also $\dot{m}_e$, ex_e, $\dot{E}x_W$, and $\dot{E}x_D$ are the outlet mass flow rate and specific exergy, exergy flows of the work, and rate of exergy destruction, respectively.

The physical exergy of a stream i is defined as follows [51,47].

$$ex = (h_i - h_0) - T_0(s_i - s_0) \quad (19)$$

In the above equation, ex, h_i, h_0, T_0, s_i, and s_0 are the specific exergy, inlet enthalpy of the enthalpy of fluid at reference conditions, ambient

temperature, entropy of stream i, and entropy at the reference condition, respectively. Table 4 shows the exergy balance equation for various components of a cycle.

Table 4. Exergy balance equations for various cyclic components.

No.	Equipment	Exergy Equation
1	Pump	$\dot{m}_1(ex_5 - ex_4) + \dot{W}_P$
2	Evaporator	$\left(\left(1-\frac{T_0}{T_E}\right)\dot{Q}_E + \dot{m}_6 ex_6\right)\left(1-\frac{T_0}{T_E}\right)\dot{Q}_E + \dot{m}_1 ex_1 - \dot{m}_6 ex_6$
3	Condenser	$\left(1-\frac{T_0}{T_C}\right)\dot{Q}_C + \dot{m}_3 ex_3 - \dot{m}_4 ex_4$
4	Internal heat exchanger	$T_0[\dot{m}_5(ex_6 - ex_5) + \dot{m}_2(ex_3 - ex_2)]$
5	Turbine	$T_0\dot{m}_1(ex_1 - ex_2) - \dot{W}_T$
6	Solar Collector	$I_g \times A\left[1+\frac{1}{3}\left(\frac{T_a}{T_{sun}}\right)^4 - \frac{4}{3}\left(\frac{T_a}{T_{sun}}\right)\right]$

In the table above, TE(K) and TC(K) are the evaporator and condenser temperatures, respectively. T_{sun} is the sun temperature of 6,000 (K), and T_{ambn}(K) is the ambient temperature.

The first and second efficiencies based on the thermodynamic laws are calculated by the subsequent relationships:

$$\eta_I = \frac{\dot{W}_T - \dot{W}_P}{\dot{Q}_E} \quad (20)$$

$$\eta_{II} = \frac{\dot{W}_T - \dot{W}_P}{I_g \times A\left[1+\frac{1}{3}\left(\frac{T_a}{T_{sun}}\right)^4 - \frac{4}{3}\left(\frac{T_a}{T_{sun}}\right)\right]} \quad (21)$$

The price of the produced electricity for the cycle is calculated by [52]:

$$C_E = \frac{CI\frac{i(1+i)^L}{(1+i)^L - 1} + C_{OM}}{8760(\dot{W}_T - \dot{W}_P)} \quad (22)$$

In the above equation, C is the initial installation cost, L is the equipment lifetime in terms of year, and i is the interest rate. The maintenance and operation costs are 4% of the initial installment cost.

The price functions of the main equipment can be calculated from table 5 [53-55].

Table 5. Cost of purchase and installation of different cycle equipment

Equipment Name	Unit	Cost function
Turbine	$	$2237(\dot{w}_T)^{0.41}$
Pump	$	$1026(\frac{\dot{W}_P}{300})^{0.25}$
Condenser	$	0338.6 A
Evaporator	$	216.6+353.4A
Solar collector	$/m^2	355

The characteristics of the working fluid are shown in table 6 [56]. The working fluid in this research work is R123. The positivity of the slope in R123 makes it possible to reduce the pressure of the condenser. In this manner, a two-phase flow cannot be produced, so there is no damage to the turbine. As a result, there is no need to superheat the fluid, resulting in low cost for evaporator due to reducing the size of the heat exchanger. For dry fluids with a positive gradient of saturated vapor curve, IHE can be used to increase the cycle efficiency. This consideration was assumed in this research work. As the pressure of the condenser is higher than the atmospheric pressure, it reduces the costs, and an ejector is not required. A higher pressure than the atmospheric pressure prevents air leakage into the system, and there is no escaping of R123 by good sealing. The low pressure of the evaporator in comparison with water is another feature of using R123, which reduces the complexity of the system. The chemical stability at high temperatures is another characteristic of using R123 as a working fluid.

Table 6. Characteristics of working fluid of ORC.

GWP (100 year)	ODP	ALT (year)	Safety degree ASHRAE	Critical Pressure (MPa)	Critical Temperature (K)	Boiling point (K)	Molecular mass $(\frac{kg}{kmol})$	Fluid
77	0.02	1.3	B1	3.662	456.83	300.97	152.93	R123

3. Multi-objective particle swarm optimization algorithm

The bird migration algorithm is a set of optimization algorithms that operate based on the random population generation. In this algorithm, the behavior of a massive group of birds or groups of fish is simulated [57-60].

Every member (particle) of this group is defined by the position vectors and velocity vector in a search space. In each iteration, the new position of the particles is defined based on the position and velocity vectors in a search space.

At each time interval, the new position of each particle is found based on the current velocity vector. Also the new position of all particle and the best position of the best particle in the group in the search domain are updated every time [57-59].

The algorithm is initially defined for the continuous and discrete parameters. This

algorithm is extended to a discrete state condition. This algorithm is also used for one or several objective functions [57-59]. Figure 3 shows a flowchart of the bird migration algorithm [61].

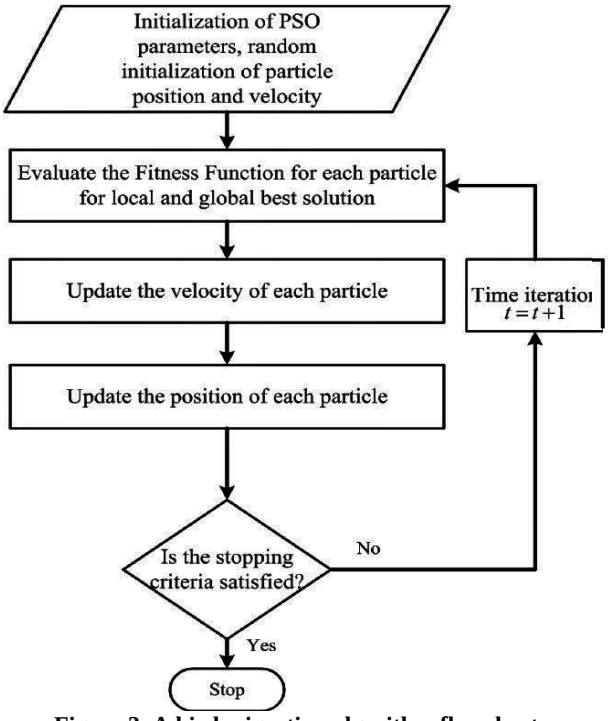

Figure 3. A bird migration algorithm flowchart.

4. Results and Discussion

In this research work, a program was written in the MATLAB software. The Refprop software was used to calculate the fluid properties. The results obtained from this work were compared with the results of the Reference [62] for validation. In this comparison, the cycle of that reference was simulated, and the results were compared. Tables 7 and 8 show the results of this comparison. Table 9 shows the values of the thermodynamic properties at different points in the cycle. The optimization process was carried out between the upper and lower limits of the variables of the cycle. The limitation of these variables is shown in table 10.

The objective function of optimization is as follows:

$$C_E \& \eta_{II} \quad [23]$$

Figure 4 represents the Pareto chart.

As it can be seen in this figure, three points are highlighted on the Pareto graph, shown as A, B, and C. Point A has the lowest electricity price and exergy efficiency, whereas point B has an average value of electricity price and exergy efficiency. Finally, point C has the highest electricity price and exergy efficiency. The other values for the points A, B, and C are presented in table 11.

Figure 5 shows the variation in the exergy and thermal efficiencies of ORC in terms of the pressure of the evaporator. As it can be seen in the figure, by increasing the pressure of the evaporator, the exergy and thermal efficiencies are increased. The exergy destruction and net produced power by ORC are shown in figure 6. Comparison of these two figures show, as the exergy destruction of the cycle is decreased, the exergy efficiency of the cycle is increased. It is also possible to observe that the cycle thermal efficiency is improved by taking the heat and increasing power production. Increasing the pressure due to the saturation state at the entrance of the turbine causes an increase in the temperature. The limiting input of hot water is one of the basic constraints in determining the pressure of the evaporator.

Figure 7 shows the exergy destruction for each component versus the evaporator pressure. It can be observed that the evaporator and condenser components have the highest exergy destruction. This is due to the entropy generation caused by the temperature difference between the hot and cold flows.

Figure 8 shows the exergy efficiency of each component. It can be observed that the two components have the highest exergy destructions, and have the lowest exergy efficiencies.

One of the economic parameters is the total annual cost for each equipment. This parameter is obtained by adding the sum of the normalized and utilization costs. The normalized cost is the cost of the equipment that is divided over the useful life of the equipment. Figure 9 shows the variation in this parameter in terms of the evaporator pressure. As the temperature of the absorbed heat in the evaporator increases, the cost of this equipment is increased too. Moreover, by increasing the pressure and temperature of the fluid flow at the turbine entrance, the cost of this equipment is increased. It can be concluded that as the evaporator pressure increases, the cost and efficiency are increased too.

Another important parameter is the pressure of the condenser. which plays a crucial character in the cycle efficiency as well as the power generation. In the cycles that deal with water and steam, the pressure of the condenser is an important parameter in increasing the lifetime of the turbine. In ORC with dry fluids, as it is stated, the turbine output is in the superheat section. As a result, this parameter can be reduced but the limitation of the cold thermal source is one of the constraints governing the condenser pressure.

In most organic fluids, which are used as refrigerants by reduction of the pressure, causes temperature reduction. Thus it requires a lower thermal resource to condense the desired fluid. As the pressure of the condenser increases, the power of the system is reduced. Thus it directly affects the exergy efficiency of the entire system, and leads to its reduction. This cycle is used just for power generation so that the exergy efficiency of the whole cycle is in agreement with the exergy efficiency of ORC. It should be noted that lower condenser temperatures are caused by lower condenser pressures (see figure 10). The reduction of the inlet temperature throughout the evaporator causes the rise of the heat absorption.

Table 7. Energy and exergy validation for this research work with Reference [62].

Points	T (ºC)		Error (%)	P (MPa)		Error (%)	ex (kJ/kg)		Error (%)
	Present study	Safarian		Present work	Safarian		Present work	Safarian	
1	25	25	0	0.044	0.048	9.0	0	0	0
2	25	26.1	4.4	2.5	2.5	0	1.84	1.77	3.8
3	50.78	55	8.3	2.5	2.5	0	3. 7	4.14	9.8
4	193.67	195	0.6	2.5	2.5	0	63.28	64.02	1.1
5	85.1	92	8.1	0.044	0.048	9.0	4.7	5.08	8.0
6	52.28	56	7.1	0.044	0.048	9.0	1.6	1.73	8.-

Table 8. Comparison of some important parameters of this research work with Reference [62].

Parameter	Unit	Present work	Safarian [62]
Evaporator heat transfer	kW	252	252
Condenser heat transfer	kW	188	196
Turbine power generation	kW	54.4	56.5
Pump power generation	kW	2.00	1.2
Net power	kW	52.37	54.3
Thermal efficiency	%	20.78	21.5
Mass flow rate (organic fluid)	kg/s	1.10	1.15

Table 9. Energy and exergy values at different points of the cycle.

Point	T (˚C)	P(kPa)	x	h (kJ/kg)	s (kJ/kg.K)	Ex (kW)
1	72.15	400	1	426.5	1.681	23.89
2	48.32	150	1>	413.4	1.691	15.54
3	39.08	150	1	406.6	1.67	15.31
4	39.08	150	0	240.9	1.139	11.41
5	39.22	400	0	241.1	1.14	11.5
6	45.67	400	0	248	1.161	11.71
7	67.78	150	0	283.7	0.9277	11.84
8	67.78	200	0	283.7	0.9277	11.84
9	89.88	150	0	376.4	1.191	26.07
Water in	25	100	0	104.8	0.367	0
Water out	35	100	0	146.6	0.505	1.455

Table 10. Upper and lower bounds of variables.

Parameter	Lower bound	Upper bound
P_E (kPa)	300	560
P_C (kPa)	145	210
Number of collector units (1.2 m^2)	100	300
Turbine isentropic efficiency	70	90
Pump isentropic efficiency	70	90

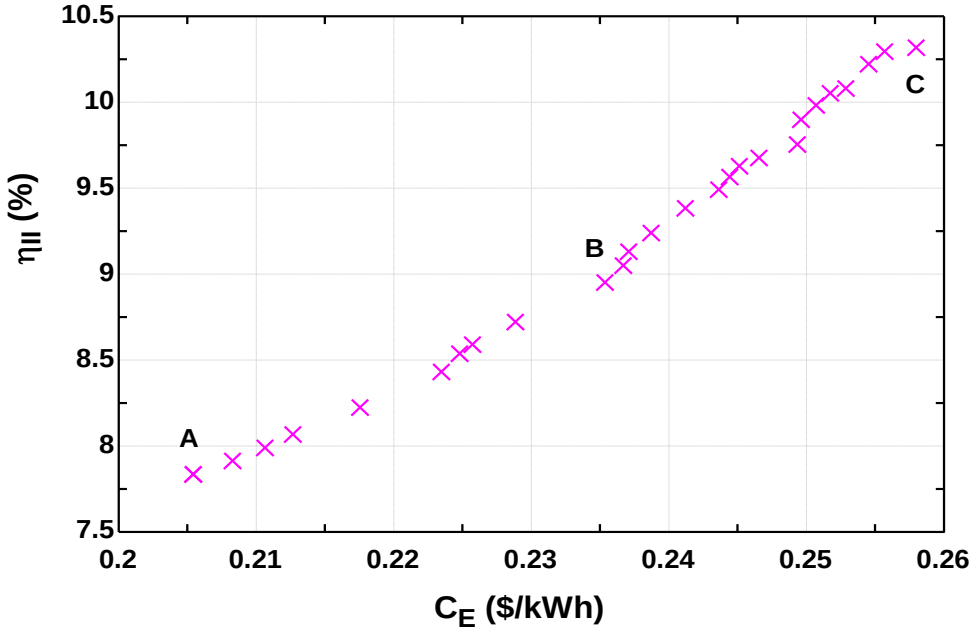

Figure 4. Pareto graph for the objective functions of exergy efficiency and the electricity price.

Table 11. Values for different variables and objective functions for points A, B, and C.

Parameter	A	B	C
P_E (kPa)	425	424.6	424.0
P_C (kPa)	145.6	145.62	145.14
Number of collector units (1.2 m^2)	247	155	111
Turbine isentropic efficiency	88.8	88.54	88.98
Pump isentropic efficiency	88.8	85.6	82.0
η_I (%)	8.42	8.36	8.39
η_{II} (%)	7.83	8.95	10.29
C_E ($/kWh)	0.2054	0.2353	0.2557

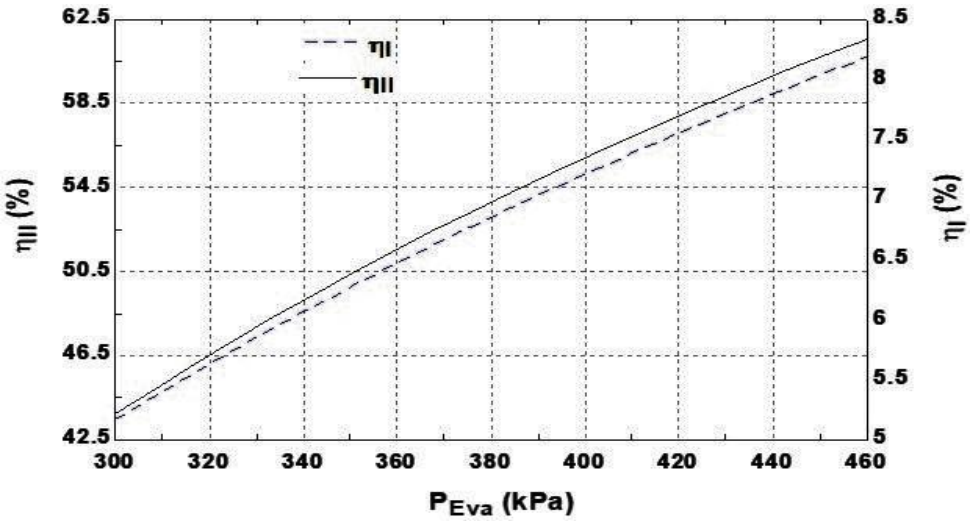

Figure 5. Changes in the energy and exergy efficiencies of ORC versus the evaporator pressure.

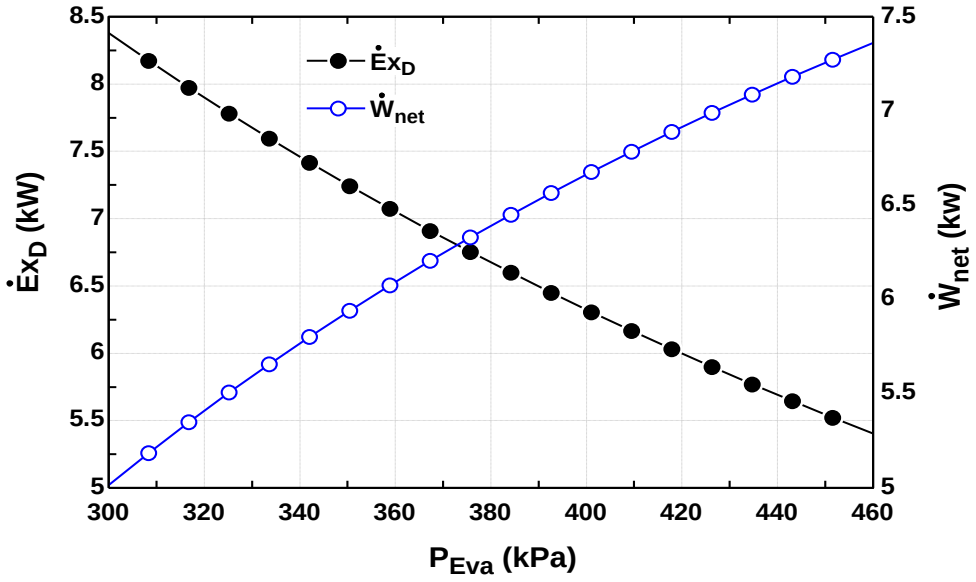

Figure 6. Changes in the exergy destruction and net produced power by ORC based on the evaporator pressure.

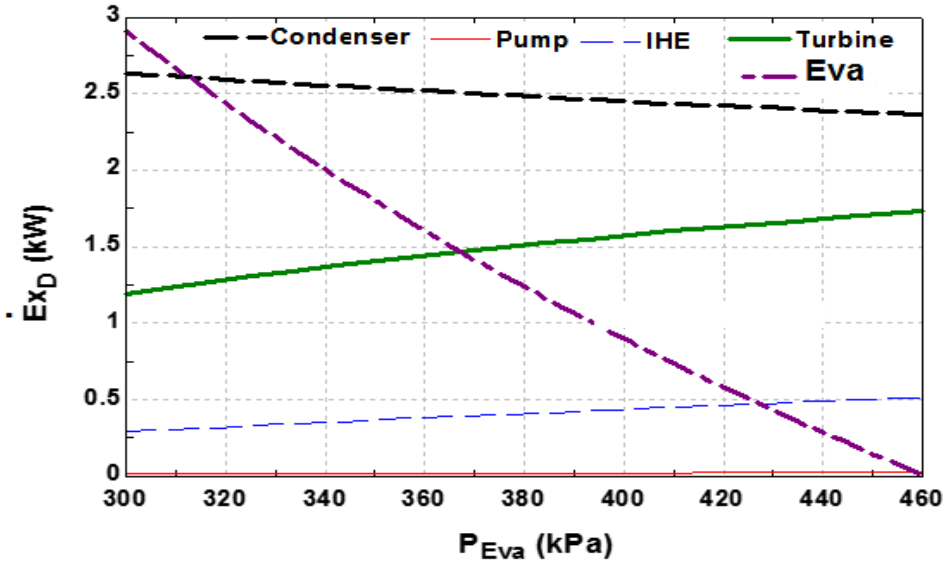

Figure 7. Changes in the exergy destruction for the ORC components based on the pressure evaporator.

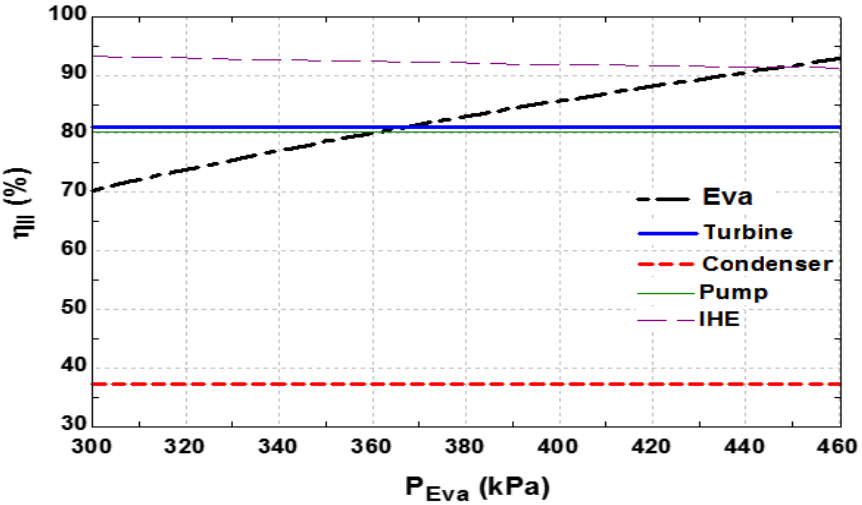

Figure 8. Exergy efficiency changes of any ORC component based on the evaporator pressure.

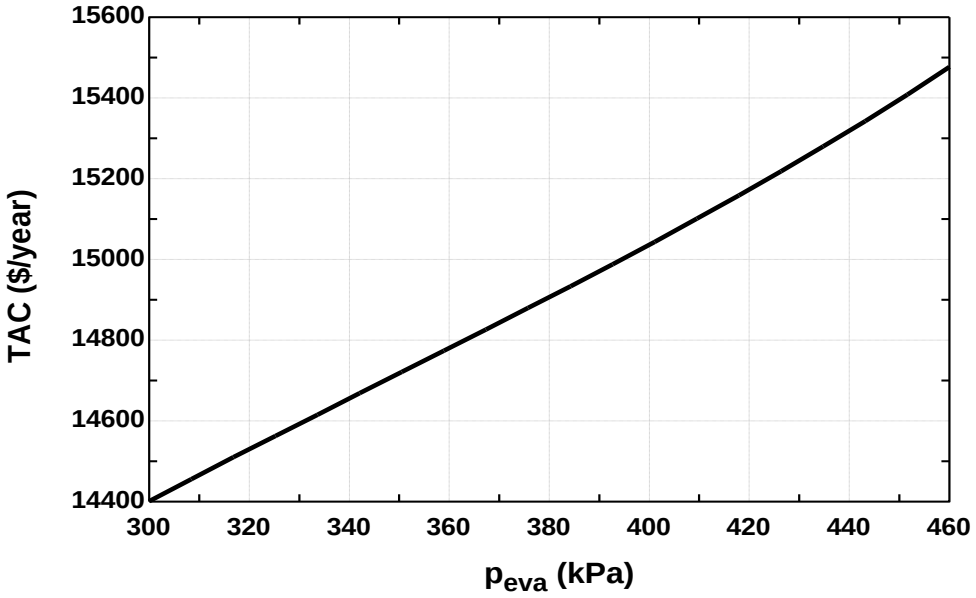

Figure 9. Changes in the total annual cost of the system with variation in the evaporator pressure.

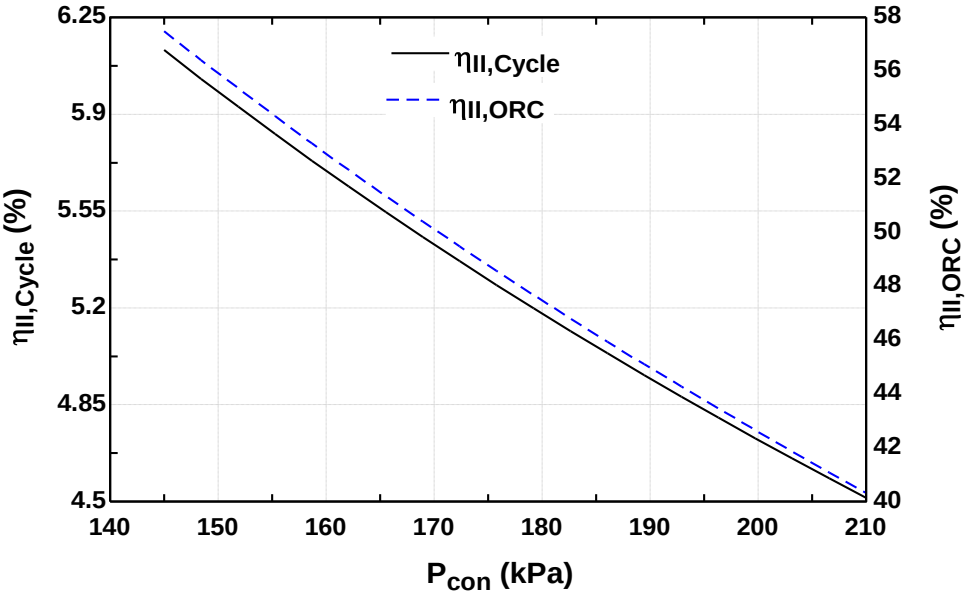

Figure 10. Changes in the total cycle and ORC exergy efficiencies.

5. Conclusion

In this research work, the application of a solar ORC with an absorption chiller to supply all energy needs (electrical, heating, and cooling) were examined. In order to comply with this goal, the energy, exergy, and economic simulations of this cycle were investigated. In the meantime, the MOPSO algorithm was applied for optimization of the purposes. In the optimization of this cycle, two objective functions consisting of exergy efficiency and electricity price were examined. In the meantime, the number of variables such as the number of solar panels, isentropic efficiencies of pump and turbine, condenser, and evaporator pressures was considered as a decision variable. The optimization results revealed that by increasing the exergy efficiency from 7.5% to 10.5%, the price of the produced electricity increased from 0.2 to 0.26 $/kWh.

The major findings of this work are as follow:

- Application of the solar ORC cycle with absorption chiller (the hybrid system in this work) can supply all the electrical, heating, and cooling loads of a system by a minimum environmental impact and clean (solar) energy;
- Two objective functions consisting of the exergy efficiency and electricity price were plotted on a Pareto-front graph in

order to find out three alternatives (highest, lowest, and medium values for the electricity price and exergy efficiency);
- The pressures of the evaporator and the condenser play an important role in the optimization of the solar ORC;
- The maximum exergy destruction rate is in the evaporator;
- For the future research works, the hydrogen and syngas production of this system by choosing the methanation plant can be used to meet the thermal energy needs of the residential building.

Abbreviations and Notations

MOPSO	Multi-objective particle swarm optimization
ORC	Organic Rankin cycle
TAC	Total annual cost

Nomenclatures

A	Surface area of collector (m^2)
c_p	Specific heat at a constant pressure (J/kg K)
C	Cost (\$), specific parameter in equation (7)
C_b	Constant parameter (-)
D_o	Tube outside diameter (m)
D_i	Tube inside diameter (m)
ex_i	Specific exergy (J/kg)
$\dot{E}x$	Exergy rate (W)
f	Specific parameter in equation (8)
F_R	Harvesting factor of the collector (-)
F'	Efficiency coefficient of the collector (-)
h	Specific enthalpy (J/kg)
h_w	Forced heat transfer coefficient (-)
h_{fi}	Heat transfer coefficient of fluid inside Tube ($W.m^{-1}.k^{-1}$)
i	Interest rate (-), inlet in equation (11)
I	Intensity of radiation (W/m^2)
K	Thermal conductivity ($W.m^{-1}.K^{-1}$)
k_T	Average monthly clearance coefficient (-)
L	Thickness or width (m), equipment lifetime (Year)
$\dot{m}$	Mass flow rate (kg/s)
m	Mass (kg)
$\dot{Q}$	Heat transfer rate (W)
R_b	Scattered radiation of the sky (-)
S	Specific entropy(J/kg.K), rate of absorbed energy(W/m^2) equation (1)
t	Time (s)
T	Temperature (˚C) or (K)
U	Heat transfer coefficient ($W.m^{-2}.K^{-1}$)
V	Velocity (m/s)
W	Distance between riser tubes (m)
$\dot{W}$	Power (W)

Subscripts

A	Ambient
B	Back
b	Below or bottom (absorbent plate)
B	Beam
C	Condenser, specific parameter in Equation (7), cost (\$) in equation (22)
D	Diffusion
d	Scattered radiation from the sky
D	Destruction
e	Sides (absorbent plate)
E	Evaporator
f	Specific parameter in equation (8)
g	Scattered radiation from the ground
H	Hot fluid
h_w	Forced heat transfer coefficient
IHE	Internal heat exchanger
L	Loss, life time (year) in equation (22)
P	Pump
sun	Sun
t	Total
T	Turbine
wind	Wind

Greek symbols

τα	Transmittance–absorptance product (-)
η	Efficiency (-)
α	Absorber coefficient (-)
β	Solar collector slope (rad)
ρ_g	Reflection coefficient of the Earth 's surface, which is equal to 0.93
ε_g	Emissivity of glass covers (-)
ε_p	Absorber plate emittance (-)
σ	Stefan–Boltzmann constant ($= 5.67 \times 10^{-8}\ W/m^2K^4$)
Θ	Angle of sunlight incidence (rad)

6. References

[1] Ahmadi A, Ehyaei MA. Development of a Simple Model to Estimate Entropy Generation of Earth.

Renewable Energy Research and Application. 2020;1(2):135-41.

[2] Majdi Yazdi MR, Ommi F, Ehyaei MA, Rosen MA. Comparison of gas turbine inlet air cooling systems for several climates in Iran using energy, exergy, economic, and environmental (4E) analyses. Energy Conversion and Management. 2020;216:112944.

[3] Ahmadi A, Esmaeilion F, Esmaeilion A, Ehyaei MA, Silveira JL. Benefits and Limitations of Waste-to-Energy Conversion in Iran. Renewable Energy Research and Application. 2020;1(1):27-45.

[4] Darvish K, Ehyaei MA, Atabi F, Rosen MA. Selection of optimum working fluid for Organic Rankine Cycles by exergy and exergy-economic analyses. Sustainability. 2015;7(1115362-83.

[5] Ehyaei MA, Ahmadi A, El Haj Assad M, Rosen MA. Investigation of an integrated system combining an Organic Rankine Cycle and absorption chiller driven by geothermal energy: Energy, exergy, and economic analyses and optimization. Journal of Cleaner Production. 2020;258:120780.

[6] R. Akbari MAE, R. Shahi Shavvon. Optimization of Solar Rankine Cycle by Exergy Analysis and Genetic Algorithm. International Journal of Energy and Power Engineering. 2019;13(9):630-7.

[7] Li Q, Beier L-J, Tan J, Brown C, Lian B, Zhong W, et al. An integrated, solar-driven membrane distillation system for water purification and energy generation. Applied Energy. 2019;237:534-48.

[8] Zhang H, Guan X, Ding Y, Liu C. Emergy analysis of Organic Rankine Cycle (ORC) for waste heat power generation. Journal of Cleaner Production. 2018;183:1207-15.

[9] Ghasemian E, Ehyaei MA. Evaluation and optimization of organic Rankine cycle (ORC) with algorithms NSGA-II, MOPSO, and MOEA for eight coolant fluids. International Journal of Energy and Environmental Engineering. 2018;9(1):39-57.

[10] Li ZX, Ehyaei MA, Kamran Kasmaei H, Ahmadi A, Costa V. Thermodynamic modeling of a novel solar powered quad generation system to meet electrical and thermal loads of residential building and syngas production. Energy Conversion and Management. 2019;199:111982.

[11] Zeinodini M, Aliehyaei M. Energy, exergy, and economic analysis of a new triple-cycle power generation configuration and selection of the optimal working fluid. Mechanics & Industry. 2019;20(5):501

[12] Ahmadi A, El Haj Assad M, Jamali DH, Kumar R, Li ZX, Salameh T, et al. Applications of geothermal organic Rankine Cycle for electricity production. Journal of Cleaner Production. 2020;274:122950.

[13] Roy JP, Mishra MK, Misra A. Parametric Optimization and Performance Analysis of a Regenerative Organic Rankine Cycle Using Low–Grade Waste Heat for Power Generation. International Journal of Green Energy. 2011;8(2):173-96.

[14] Wang ZQ, Zhou NJ, Guo J, Wang XY. Fluid selection and parametric optimization of organic Rankine cycle using low temperature waste heat. Energy. 2012;40(1):107-15.

[15] Badr O, O'callaghan P, Probert S. Rankine-cycle systems for harnessing power from low-grade energy sources. Applied Energy. 1990;36(4):263-92.

[16] Maizza V, Maizza A. Unconventional working fluids in organic Rankine-cycles for waste energy recovery systems. Applied thermal engineering. 2001;21(3):381-90.

[17] Liu B-T, Chien K-H, Wang C-C. Effect of working fluids on organic Rankine cycle for waste heat recovery. Energy. 2004;29(8):1207-17.

[18] Drescher U, Brüggemann D. Fluid selection for the Organic Rankine Cycle (ORC) in biomass power and heat plants. Applied thermal engineering. 2007;27(1):223-8.

[19] Yousefi M, Ehyaei MA. Feasibility study of using organic Rankine and reciprocating engine systems for supplying demand loads of a residential building. Advances in Building Energy Research. 2019;13(1):32-48.

[20] Heberle F, Preißinger M, Brüggemann D. Zeotropic mixtures as working fluids in Organic Rankine Cycles for low-enthalpy geothermal resources. Renewable Energy. 2012;37(1):364-70.

[21] Li W, Feng X, Yu L, Xu J. Effects of evaporating temperature and internal heat exchanger on organic Rankine cycle. Applied Thermal Engineering. 2011;31(17-1 4014-23.

[22] M.A.Ehyaei HKa. Energy, exergy, and economic analysis of a geothermal powerplant. Advances inGeo-Energy Research. 2018;2(2):190-209.

[23] Quoilin S, Orosz M, Hemond H, Lemort V. Performance and design optimization of a low-cost solar organic Rankine cycle for remote power generation. Solar Energy. 2011;85(5):955-66.

[24] Ben Youssef W, Maatallah T, Menezo C, Ben Nasrallah S. Modeling and optimization of a solar system based on concentrating photovoltaic/thermal collector. Solar Energy. 2018;170:301-13.

[25] Karellas S, Schuster A, Leontaritis A. Influence of supercritical ORC parameters on plate heat exchanger design. Applied Thermal Engineering. 2012;s 33–34:70–6.

[26] Chen H, Goswami D, Rahman M, K. Stefanakos E. Energetic and exergetic analysis of CO2- and R32-based transcritical Rankine cycles for low-grade heat conversion. Applied Energy. 2011;88:2802-8.

[27] Chen H, Goswami D, Rahman M, K. Stefanakos E. A supercritical Rankine cycle using zeotropic mixture working fluids for the conversion of low-grade heat into power. Fuel and Energy Abstracts. 2011;36:549-55.

[28] Wang H, Peterson R, Harada K, Miller E, Ingram-Goble R, Fisher L, et al. Performance of a combined organic Rankine cycle and vapor compression cycle for heat activated cooling. Energy. 2011;36(1):447-58.

[29] Wang M, Wang J, Zhao Y, Zhao P, Dai Y. Thermodynamic analysis and optimization of a solar-driven regenerative organic Rankine cycle (ORC) based on flat-plate solar collectors. Applied Thermal Engineering. 2013;50(1):816-25.

[30] Baccioli A, Antonelli M, Desideri U. Dynamic modeling of a solar ORC with compound parabolic collectors: Annual production and comparison with steady-state simulation. Energy Conversion and Management. 2017;148:708-23.

[31] Bellos E, Tzivanidis C. Investigation of a hybrid ORC driven by waste heat and solar energy. Energy Conversion and Management. 2018;156:427-39.

[32] Saadatfar B, Fakhrai R, Fransson T. Conceptual modeling of nano fluid ORC for solar thermal polygeneration. Energy Procedia. 2014;57:2696-705.

[33] Mokhtari H, Ahmadisedigh H, Ebrahimi I. Comparative 4E analysis for solar desalinated water production by utilizing organic fluid and water. Desalination. 2016;377:108-22.

[34] Zhang Y, Deng S, Zhao L, Ni J, Ma M, Lin S, et al. Clarifying the bifurcation point on Design: A Comparative Analysis between Solar-ORC and ORC-based Solar-CCHP. Energy Procedia. 2017;142:1119-26.

[35] Patel B, Desai NB, Kachhwaha SS, Jain V, Hadia N. Thermo-economic analysis of a novel organic Rankine cycle integrated cascaded vapor compression–absorption system. Journal of Cleaner Production. 2017;154:26-40.

[36] Mohammadi A, Mehrpooya M. Thermodynamic and economic analyses of hydrogen production system using high temperature solid oxide electrolyzer integrated with parabolic trough collector. Journal of Cleaner Production. 2019;212:713-26.

[37] Ashari GR, Ehyaei MA, Mozafari A, Atabi F, Hajidavalloo E, Shalbaf S. Exergy, Economic, and Environmental Analysis of a PEM Fuel Cell Power System to Meet Electrical and Thermal Energy Needs of Residential Buildings. Journal of Fuel Cell Science and Technology. 2012;9(5).

[38] Mohammadnezami MH, Ehyaei MA, Rosen MA, Ahmadi MH. Meeting the Electrical Energy Needs of a Residential Building with a Wind-Photovoltaic Hybrid System. Sustainability. 2015;7(3):2554-69.

[39] Yousefi M, Ehyaei MA, Rosen MA. Optimizing a New Configuration of a Proton Exchange Membrane Fuel Cell Cycle With Burner and Reformer Through a Particle Swarm Optimization Algorithm for Residential Applications. Journal of Electrochemical Energy Conversion and Storage. 2019;16(4).

[40] Aliehyaei M, Atabi F, Khorshidvand M, Rosen MA. Exergy, Economic and Environmental Analysis for Simple and Combined Heat and Power IC Engines. Sustainability. 2015;7(4):4411-24.

[41] Naseri A, Fazlikhani M, Sadeghzadeh M, Naeimi A, Bidi M, Tabatabaei SH. Thermodynamic and Exergy Analyses of a Novel Solar-Powered CO2 Transcritical Power Cycle with Recovery of Cryogenic LNG Using Stirling Engines. Renewable Energy Research and Application. 2020;1(2):175-85.

[42] https://weatherspark.com/y/105125/Average-Weather-in-Tehran-Iran-Year-Round [Access 2019].

[43] Kalogirou SA. Solar thermal collectors and applications. Progress in Energy and Combustion Science. 2004;30(3):231-95.

[44] Mokhtari H, Ahmadisedigh H, Ameri M. The optimal design and 4E analysis of double pressure HRSG utilizing steam injection for Damavand power plant. Energy. 2017;118:399-413.

[45] Bergman TL, Incropera FP, Lavine AS, Dewitt DP. Introduction to heat transfer: John Wiley & Sons, 2011.

[46] Hajabdollahi H. Evaluation of cooling and thermal energy storage tanks in optimization of multi-generation system. Journal of Energy Storage. 2015;4:1-13.

[47] Cengel YA, Boles MA. Thermodynamics: an engineering approach. Sea. 2002;1000:8862.

[48] Mozafari A, Ehyaei MA. Effects of Regeneration Heat Exchanger on Entropy, Electricity Cost, and Environmental Pollution Produced by Micro Gas Turbine System. International Journal of Green Energy. 2012;9(1):51-70.

[49] Asgari E, Ehyaei MA. Exergy analysis and optimisation of a wind turbine using genetic and searching algorithms. International Journal of Exergy. 2015;16(3):293-314.

[50] Shaygan M, Ehyaei MA, Ahmadi A, Assad MEH, Silveira JL. Energy, exergy, advanced exergy and economic analyses of hybrid polymer electrolyte membrane (PEM) fuel cell and photovoltaic cells to produce hydrogen and electricity. Journal of Cleaner Production. 2019;234:1082-93.

[51] Ehyaei MA, Ahmadi A, Assad MEH, Hachicha AA, Said Z. Energy, exergy and economic analyses for the selection of working fluid and metal oxide nanofluids in a parabolic trough collector. Solar Energy. 2019;187:175-84.

[52] Frangopoulos CA. Thermo-economic functional analysis and optimization. Energy. 1987;12(7):563-71.

[53] Alshammari F, Karvountzis-Kontakiotis A, Pesyridis A, Usman M. Expander Technologies for Automotive Engine Organic Rankine Cycle Applications. Energies. 2018;11(7):1905.

[54] Lecompte S, Huisseune H, Van den Broek M, De Schampheleire S, De Paepe M. Part load based thermo-economic optimization of the Organic Rankine Cycle (ORC) applied to a combined heat and power (CHP) system. Applied Energy. 2013;111:871-81.

[55] Quoilin S, Declaye S, Tchanche BF, Lemort V. Thermo-economic optimization of waste heat recovery Organic Rankine Cycles. Applied thermal engineering. 2011;31(14-15):2885-93.

[56] Brown JS. HFOs: new, low global warming potential refrigerants. Ashrae Journal. 2009;51(8):22-8.

[57] Eberhart R, Kennedy J. A new optimizer using particle swarm theory. Conference A new optimizer using particle swarm theory. IEEE, p. 39-43.

[58] Eberhart RC, Shi Y. Comparison between genetic algorithms and particle swarm optimization. Conference Comparison between genetic algorithms and particle swarm optimization. Springer, p. 611-6.

[59] Coello CAC, Pulido GT, Lechuga MS. Handling multiple objectives with particle swarm optimization. IEEE Transactions on evolutionary computation. 2004;8(3):256-79.

[60] Shirmohammadi R, Ghorbani B, Hamedi M, Hamedi M-H, Romeo LM. Optimization of mixed refrigerant systems in low temperature applications by means of group method of data handling (GMDH). Journal of Natural Gas Science and Engineering. 2015;26:303-12.

[61] Clerc M. Particle-Swarm Optimization (iste ed.). London; 2006.

[62] Safarian S, Aramoun F. Energy and exergy assessments of modified Organic Rankine Cycles (ORCs). Energy Reports. 2015;1:1-7.